Materials Horizons

ROYAL SOCIETY OF CHEMISTRY

COMMUNICATION

View Article Online
View Journal | View Issue

Cite this: *Mater. Horiz.*, 2023, **10**, 2989

Received 21st December 2022,
Accepted 9th May 2023

DOI: 10.1039/d2mh01553f

rsc.li/materials-horizons

Frontally polymerized foams: thermodynamic and kinetical aspects of front hindrance by particles†

Petr Lepcio,[a] John Daguerre-Bradford,[b] Anna Maria Cristadoro,[c] Markus Schuette[c] and Alan J. Lesser*[b]

Frontal polymerization (FP) is a solvent-free, energy-efficient process where a self-propagating polymerization reaction with a characteristic sharp temperature gradient at the front head propagates through the resin to provide the curing conditions. It relies on the enthalpic balance, which spreads the reaction to unreacted resin in the neighborhood. Therefore, the FP is sensitive to the presence of non-reactive volumes, such as boundaries, fillers, or other additives, that retain heat from the front but produce no enthalpy in return. On the other hand, the front's high temperature could be used to initiate other processes, such as foaming, incorporating them into a simple single-step fabrication procedure. This study used silica particles of two different sizes (14 nm and 200–300 nm) in an epoxy-based FP foam as a representative filler to probe the constraints imposed by non-reactive additives. The presence of particles visibly hindered the front propagation, increased the foam density and even corrupted the frontal regime in some cases. We show that preheating or chemical composition changes are viable approaches to address the fillers' adverse effects. Furthermore, we present evidence that the reduced reaction enthalpy caused by silica nanoparticles, was balanced by the lower heat capacity of our model system. At the same time, the front hindrance was attributed to changes in reaction kinetics and the heat distribution around the front. These results set up essential narratives for the design and practical applications of frontally polymerized foams with non-reactive fillers.

New concepts

This manuscript establishes basic narratives for designing and implementing fillers in frontally polymerized (FP) foams. New fundamental insights into the thermodynamics and kinetical effects induced by micro- and nanoparticles to frontal polymerization are presented. FP foams are favored for energy-efficient curing, high conversion, and good mechanical performance. However, adding particles to an FP formulation may require adjustments to maintain the frontal regime of polymerization by restoring the enthalpic balance. The three main phases of FP are the preheating ahead of the front, the front head with maximum temperature, and the heat retention after the front passes. All three processes are significantly affected by the presence of particles. We demonstrate new design strategies addressing these challenges preventing this field from further expansion. Either the formulation could be preheated before the initiation, the reaction rate can be accelerated by adding more initiator, or the reaction enthalpy might be increased by adjusting the monomer composition. These results open a way toward innovative composite and nanocomposite FP foams. This new class of materials can combine simple and efficient processing, lightweight structure, mechanical robustness, and advanced properties, such as thermal or electrical conductivity, introduced by functional nanofillers.

1. Introduction

Frontal polymerization (FP) is a special polymerization process where once initiated at one location, can propagate from the initiation site through the volume of the uncured resin *via* the exotherm generated during the cure. As the curing proceeds, the evolving excess heat locally self-initiates the reaction in nearby regions. This process is repeated until the propagating polymerization creates a front with a characteristic sharp temperature gradient. These curing conditions are far more energy efficient than thermal curing[1] while not suffering from the short pot-life of chemically cured formulations.[2] At the same time, the solvent-free FP conditions generate minimum waste and offer specific unique properties compared to bulk polymerization, such as higher conversion, better mechanical performance, or chemical resistance.[3] Moreover, the front could initiate other processes such as in-situ synthesis of nanoparticles[4] or foaming.[5] These parameters make the FP a good candidate for environmentally friendly and sustainable processing methods, especially in combination with green chemistries.[6,7]

[a] *Central European Institute of Technology, Brno University of Technology, Purkyňova 656/123, 612 00 Brno, Czech Republic*
[b] *University of Massachusetts Amherst, 120 Governors Drive, Amherst, MA 01003, USA. E-mail: petr.lepcio@ceitec.vutbr.cz*
[c] *BASF Polyurethanes, Elastogranstr 60, Lemfoerde, 49448, Germany*

† Electronic supplementary information (ESI) available: The supporting information file contains additional data with a frontal regime corrupted by particles, a raw DSC curve, and temperature profiles of the filled samples. See DOI: https://doi.org/10.1039/d2mh01553f

The frontal regime is governed by the enthalpic balance between heat generation, consumption, and losses to the environment and simultaneous processes.[2] The heterogeneous materials near the reaction front may absorb and retain the excess reaction enthalpy while producing no reaction enthalpy in return. Hence, the FP is sensitive to boundary conditions and unreactive volume, *e.g.*, fillers. Even a tiny variation of activation energy may have a prominent effect on the front velocity and limit the maximum content of unreactive additives eligible for achieving the FP conditions.[8] Insufficient, slow, or uneven heat evolution causes the front to cool down and decelerate; it may result in fingering or even disrupt the self-propagation.[9,10] This could also originate from the increased cross-linking density or slower diffusion in the system.[2] On the other hand, too large excess heat promotes self-initiation, and the reaction becomes more similar to standard bulk polymerization.[11]

Nanoparticles and other nanomaterials represent a specific category of fillers with pronounced interfacial effects.[12] They are favored for nanoreinforcement,[13] functional additivation,[14,15] and, generally, a simple modification of properties.[16] Davtyan, *et al.* reported an almost negligible effect of silica nanoparticles (NPs) on the front propagation and temperature of PMMA/methyl methacrylate solution up to the concentration corresponding to the NP aggregation limit.[17] On the other hand, larger or aggregated particles caused a far more pronounced front hindrance. Interestingly, Davtyan, *et al.* also documented an improved NP dispersion after the FP. A strong shear field is usually required to achieve a good NP dispersion, *e.g.*, in a twin screw extruder[18] or ultrasonication-induced cavitation.[19,20] Nanosilica particles were also found to stabilize the front and suppress fingering.[9] Such observation has great practical importance because the quality of NP dispersion directly influences the material properties.[21] For instance, the mechanical and thermal properties stem from the immobilized and frustrated polymer layer adsorbed around the NPs[22] that experience the nanoconfinement effect.[23]

Finally, nanocomposite foams represent a broad category of lightweight materials. NPs and other nanofillers are often used to control the foam morphology, reducing the cell size through enhanced cell nucleation[24–26] or introducing functional properties such as electric conductivity.[27] However, NPs also have a complex effect on mechanical deformation and fracture due to the combined nanoconfinement effect from soft and stiff inclusions represented by the voids and the nanoparticles.[26] In the only previous attempt known to the authors, the FP has been deployed to fabricate polymer foams by including a physical blowing agent into a standard FP formulation.[5] The morphology of FP foams was controlled by the concentration and type of the blowing agent. At the same time, the temperature and viscosity gradient at the front head resulted in a prominent anisotropy of the foam cells.[5] We note that this single-step procedure might be better suited for fabricating anisotropic foams at a large scale than the templating processes.[28] Nonetheless, the vaporization of a physical blowing agent retained heat from the front, compromising its stability.[5] This factor limits the versatility of this approach, especially in combinations with other non-reactive additives.

Instead, an exothermic chemical blowing agent may prove a more viable solution for achieving low foam density and a high polymerization rate. The current study presents frontally polymerized foams based on a thermosetting epoxy resin. An azodicarbonamide-based blowing agent started the foaming near the polymerization temperature, and two sizes of silica particles (14 nm and 200–300 nm) were used as representative filler. The particles caused an apparent front hindrance manifested by a slower front propagation rate and increased foam density. A detailed insight into the thermodynamics by modulated DSC suggested that the nanoparticles lowered the reaction heat. Yet, it was countered by the reduced heat capacity of the nano-filled formulation. Thus, the crucial role in the front hindrance was attributed to reaction kinetics and heat distribution around the front. Thermal imaging was used to evaluate the front temperature gradients, to separate the contributions in three regions – preheating ahead of the front, the front head with maximum temperature, and the heat retention after the front passes. All three regions were significantly affected by the presence of particles. The presented results set up basic narratives for the design and implementation of nanoparticles into the frontally polymerized foams.

2. Materials and methods

Materials

The basic FP formulation used in this study is a patented technology of the BASF company and the University of Massachusetts Amherst. The main components were the 3,4-epoxycyclohexylmethyl 3,4-epoxycyclohexanecarboxylate (ECC, Sigma Aldrich, Germany) and bisphenol A diglycidyl ether (DGEBA, Olin Epoxy, USA) monomers in the ratio of 60 : 40. It further contained 2.5% of the *p*-(octyloxyphenyl)phenyliodonium hexafluoroantimonate (IOC, Gelest, USA) photoinitiator, 2.5% of the 1,1,2,2-tetraphenyl-1,2-ethanediol (Sigma Aldrich, Germany), 0.5% of the azodicarbonamide based RAZ-P foaming agent (Reedy Chemicals, USA), and 1% of the DC-193 stabilizer (Dow Silicon, USA). The 3% IOC and 70 : 30 ECC : DGEBA samples were varied from the basic FP formulation by adjusting the IOC concentration and the monomer ratio, respectively. Silica particles with an average size of 14 nm and 200–300 nm were supplied from Sigma Aldrich (Germany) and used as obtained.

Sample preparation

All components of the FP formulation were mixed and stirred for 1 hour at 60 °C. Particles were then added and homogenized with a Branson Sonifier 450 (USA) for 4 minutes at 20% duty cycle and the power set to 6. The formulation was poured into a 2 × 2″ pre-cut rubber mold placed on a PTFE sheet and initiated by a hot soldering iron (Weller WP 80, 80 W, 24 V, setpoint 250 °C). The front propagated in the horizontal direction with no upper boundary.

Characterization

The foam density was measured using water as a working medium with a pycnometer. The reaction enthalpy was measured by a DSC Q200 (TA Instruments, USA) in hermetic pans at a heating ramp of 10 °C min^{-1}. Modulated DSC (M-DSC) was performed with the same instrument at the heating ramp of 2 °C min^{-1}, modulation amplitude of 0.5 °C, and a period of 60 s. The filler concentration was evaluated by TGA (Q50, TA Instruments, USA) from the residual weight after a 10 minute hold at 700 °C. The results were corrected on the unfilled formulation's residual weight of 0.48%. Magellan 400 (FEI, Czech Republic) collected the SEM images using a secondary electron detector on gold-coated samples at the acceleration voltage of 2 kV.

Thermal imaging was performed with a FLIR A325sc thermal camera on a front propagating through a 1 × 5″ mold. The maximum temperature and temperature profiles were analyzed using the FLIR tools OEM software. The preheating and cooling rate was evaluated by a linear fit of 7 different spots in the range of 37.5–100 °C and 40 °C beyond the front temperature, respectively. Front velocity was calculated from the peak temperature time and the known distance of the selected points.

3. Results and discussion

The foam density is a basic property that can be related to the engineering properties of the foam through micromechanics as well as other physical properties. These will be discussed in a separate publication, and it is not the focus of the current investigation. For the model system presented herein, it was established as 0.569 g cm^{-3} (Fig. 1). These FP foams feature a tough skin layer near the boundaries with a relatively smooth surface on top and the skin layer roughness on the bottom being a function of the substrate the foam is generated on. In contrast, the actual density of the foamed core is much lower. Adding silica particles visibly hinders the front propagation and increases the density of the foams. 1 vol% of the 14 nm silica nanoparticles slow the reaction to the point that the front cannot form at laboratory temperature. Only a tiny area near the hot tip is cured (Fig. S1, ESI†). In this case, the frontal regime can only be achieved by preheating the formulation in an oven to 60 °C before the initiation. These results contradict Davtyan's conclusions that nanoparticles have negligible impact on the front propagation.[17]

Two strategies are employed to bring the filled foams' densities down to the level of the basic formulation. Firstly, the reaction rate is enhanced by increasing the IOC initiator

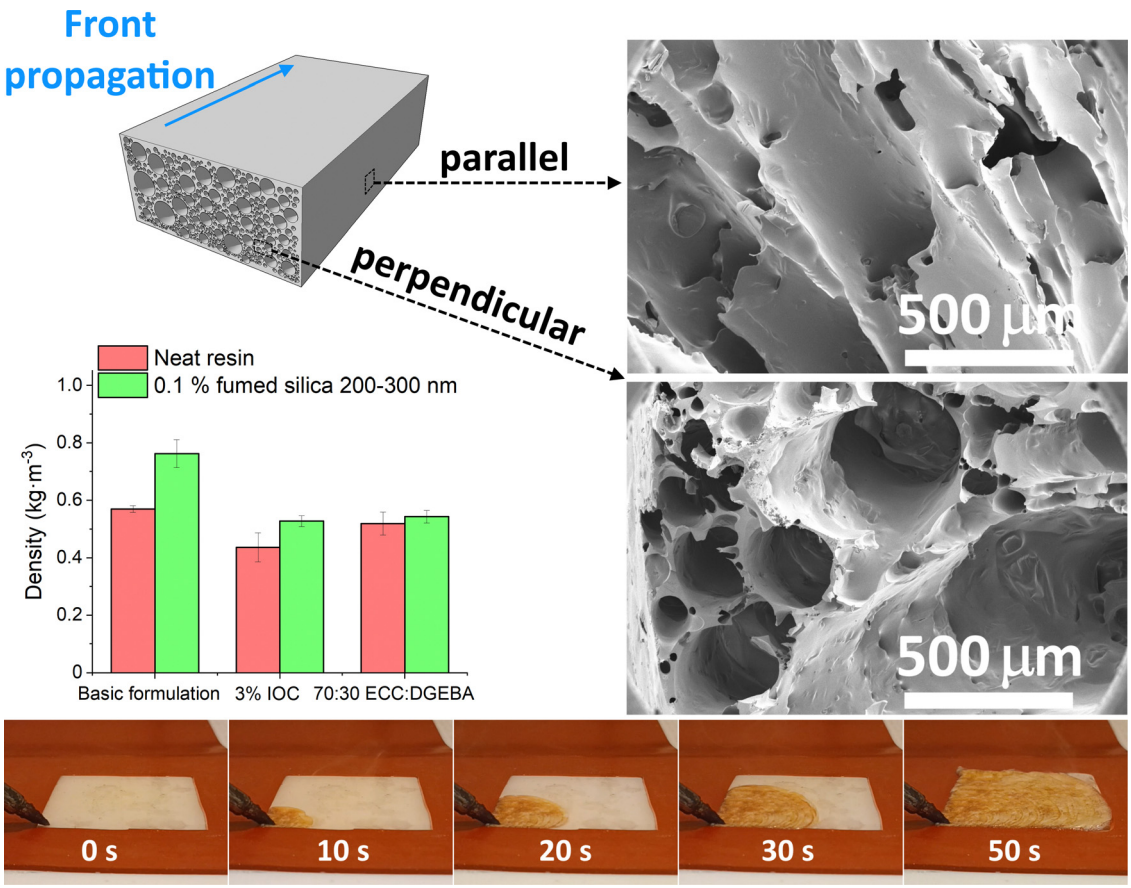

Fig. 1 Frontally polymerized foams. SEM images of the porosity in parallel (top right) and perpendicular (middle right) directions respective to the front propagation. The density of the selected samples measured by a pycnometer (middle left). Images of the propagating front in time (bottom).

concentration from 2.5 to 3%, assuming that the total reaction enthalpy remains nearly unchanged thanks to the high monomer conversions achieved by frontal polymerization.[3] Secondly, the reaction enthalpy is boosted by adjusting the monomer ratio from 60 : 40 to 70 : 30 ECC : DGEBA. We note that the densities of unfilled foams also decrease in both cases (Fig. 1).

The critical parameter of all FP chemistries is maintaining the front's enthalpic balance. Thus, the reaction enthalpies are measured by DSC (Fig. S3 left, ESI†). An entire DSC curve for the standard FP foam formulation is displayed in Fig. S3 (ESI†) right. It was previously reported that the reaction enthalpy violates the simple rule of mixture.[2] Instead, the mixture properties are predicted to lie between an upper bound defined by the weighted arithmetic mean (WAM) and a lower bound based on each component's weighted harmonic mean (WHM).[2] Moreover, the temperature ramp test and the small reaction volume used for this measurement might not capture the frontal conditions, yet we assume that the reaction enthalpies scale accordingly. Nonetheless, the enthalpy recorded for the 70 : 30 ECC:DGEBA sample (508 J g^{-1}) is nearly identical to the basic formulation (516 J g^{-1}) while the 3% IOC has even lower value (486 J g^{-1}, Fig. S3 left, ESI†). Interestingly, this trend is discontinued in the samples filled with 0.1% of 200–300 nm fumed silica. Instead, their enthalpies scale in the order Basic formulation (437 J g^{-1}) < 3% IOC (477 J g^{-1}) ≈ 70 : 30 ECC : DGEBA (469 J g^{-1}), corresponding well to their densities (Fig. 1).

While these results appear confusing, there are several processes going on simultaneously, which the standard DSC cannot distinguish. Moreover, the baseline of the heat flow curve shifts as the heat capacity changes throughout the reaction. On the other hand, a modulated DSC (M-DSC) can separate the contributions of reversible and irreversible enthalpies (Fig. 2). Repeating the test several times while omitting varying components of the formulation identifies the individual peaks (Fig. S2, ESI†). The three most pronounced processes are associated with the ECC and DGEBA polymerization, which shall be treated separately,[29] and the decomposition of the foaming agent (Fig. 2). Glass transition, ECC evaporation peak, and the changes in heat capacity throughout the reaction (Fig. 2) are recognized in the much weaker reversible heat flow signal.

Polymerization is the first process starting at the lowest temperature (around 80 °C). The glass transition, which follows at 97 °C for the standard formulation, is expected in this range for an epoxy resin.[30] An irreversible exothermic peak of foaming appears with a maximum at 116.9 °C. Finally, the lighter and more reactive ECC monomer ceases reaction at roughly 160 °C, while the heavier and less reactive DGEBA monomer reacts until roughly 220 °C. The results correlate well with the expectation that the heavier monomer's reaction is slower than the lighter one's.[29] The reversible enthalpy peak at 116.3 °C is attributed to the ECC evaporation (boiling point 170 °C) because it is still present even in the absence of the foaming agent. Yet, it is probably no coincidence that this peak aligns near the maximum of the highly exothermic foaming (Fig. 2).

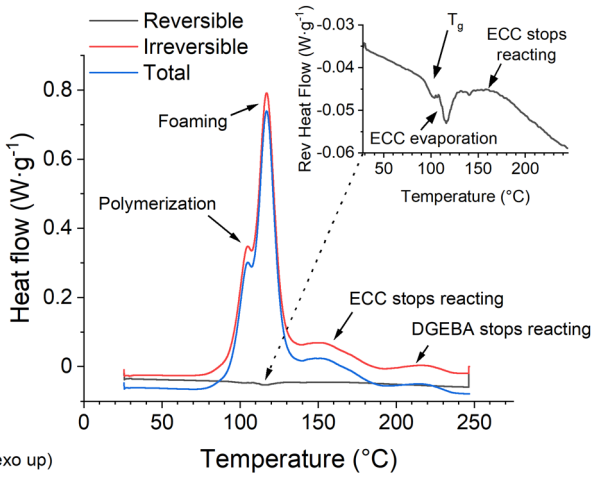

Fig. 2 Total, reversible, and irreversible heat flow curve of the FP formulation obtained by the modulated DSC. The inset shows an enlarged detail of the reversible heat flow in the range of the reaction.

Further experiments are performed with the 3% IOC sample because the standard formulation cannot frontally polymerize in the presence of particles at the tested boundary conditions. Adding 1 vol% of 14 nm silica nanoparticles is a representative example probing the effect of filling. The recorded enthalpies (total, reversible, irreversible), glass transition, and heat capacity at 50 °C for both samples are listed in Table S1 (ESI†). The results are quite sensitive to the precise composition and the monomer ratio, which is affected by the ECC evaporation upon processing. Therefore, the filled and unfilled samples are prepared from a single batch and processed together to achieve high precision. Notably, the unfilled formulation is also ultrasonicated, although it has no practical meaning beyond maintaining the same processing conditions. Silica nanoparticles slightly influence the irreversible enthalpy (Fig. S4 left, ESI†). The recorded change of 18.7 J g^{-1} represents a decrease of 3.1%, exceeding the expectation based on the simple volume replacement (Table S1, ESI†). While the onset of polymerization is slightly hindered, the exothermic foaming peak is more pronounced (Fig. S4 left, ESI†). A possible explanation is the nanoparticle's capability to catalyze the decomposition of the foaming agent,[31] but it could also increase due to the delayed curing.[32] The final part of the ECC and DGEBA reactions are practically independent of the filling (Fig. S4 left, ESI†).

The T_g of the 3% IOC is observed at a lower temperature (95 °C, Fig. S4 right, ESI†) than in the standard formulation (97 °C, Fig. 2) due to its faster curing. The filling was indifferent to T_g within the experimental error, keeping the value of 95 °C (the device's temperature accuracy is ±0.05 °C and the temperature precision is ±0.1 °C). The peak attributed to ECC evaporation is also pronounced by adding nanoparticles (Fig. S4 right, ESI†), presumably due to the particle nucleation effect, which eases the monomer evaporation. Nonetheless, the most pronounced difference is the shift of the filled sample's baseline towards higher (less negative) levels of the reversible heat flow (Fig. S4 right, ESI†). The baseline represents the heat

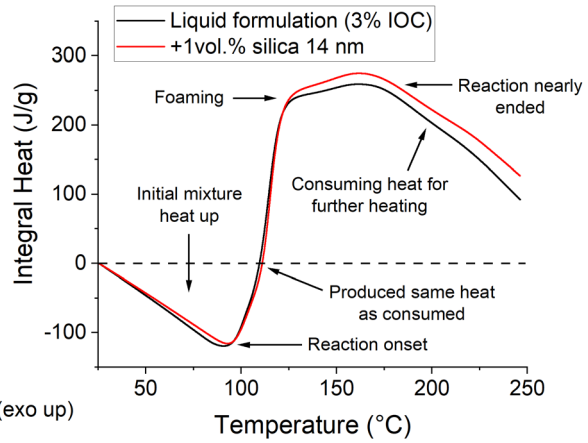

Fig. 3 Integral curves comparing the heat consumption and evolution of the FP formulations as a function of temperature.

consumed by the sample's heating and directly corresponds to its heat capacity. The upshift manifests a drop in the heat capacity of the filled sample from 1.927 J g^{-1} K^{-1} (measured at 50 °C) to 1.775 J g^{-1} K^{-1}, because it requires less enthalpy for heating. Silica and other oxidic nanoparticles adhere well to hydrophilic matrices,[33] leading to the well-known nanoreinforcement effect,[23] increased viscosity,[34] and the stiffening of the formulation. In turn, a lower heat capacity is generally expected from a more solid-like material due to the suppressed inner motion. Nonetheless, it is essential to highlight that the lower heat capacity fully compensates the losses in curing enthalpy caused by the volume replacement. This principle may explain the previously reported zero effect of nanoparticle additives on frontal polymerization at low particle concentrations.[17]

The integral heat curves, *i.e.*, the heat curves integrated over the temperature (Fig. 3), clearly document this phenomenon. The process starts with a heat consumption required for the initial heat-up, and the trend only turns upwards to become exothermic at the reaction onset (92.7 and 90.7 °C for the filled and unfilled samples, respectively). The reaction enthalpy contributes the same heat as required for the initial heating phase at around 110 °C. This point marks the minimum temperature which must be theoretically reached by the front's head to sustain the front. Though, the heat retention and losses push this point to higher temperatures in real samples. Nonetheless, the reaction continues until the maximum excess heat is obtained near the temperature where the ECC stops reacting with a distinct shoulder around the foaming temperature (Fig. 3). Finally, the heat consumption phase is recovered when the reaction enthalpy is (nearly) exhausted.

The integral curves for the filled and unfilled samples are nearly identical up to approx. 125 °C, while a discrepancy develops above this temperature (Fig. 3). The filled formulation evolves more excess heat per unit weight, which could be distributed into the neighboring areas to propagate the front. The importance of the lowered heat capacity is superior to the reduced reaction enthalpy (Table S1, ESI†). It is unclear how much this conclusion relates to this specific case and could be generalized to other nano-filled FP formulations. Nonetheless, the results seemingly disapprove our initial observation that nanoparticles hinder the front propagation while supporting the conclusion of Davtyan, *et al.*[17] An apparent drawback of the low enthalpy-low capacity case is its higher sensitivity to boundary conditions. The boundaries take away the same amount of heat (at a given temperature), yet the filled formulation must donate it by reacting larger mass/volume than the unfilled one. Nevertheless, a potential explanation of the observed difference may be found in the curing kinetics. Free-radical polymerization of acrylics, used by Davtyan, *et al.*,[17] generally provide a faster curing reaction than catatonically polymerized epoxies used in this study. Moreover, Davtyan, *et al.* used a simple frontal polymerization, but the azodicarbonamide foaming agent decomposition may also interact with the nanoparticles.[31] Indeed, our further evidence suggests that the hindrance effect should be related to kinetics rather than thermodynamics, as initially assumed.

The kinetics are assessed by thermal imaging of the propagating front over a distance of 5″. The maximum temperature sensed by the camera in the whole thermal image (Fig. 4 left) and temperature profiles at several fixed points (Fig. 4 right) are evaluated. The peak temperature times of the individual points are combined with their known distance to obtain the front velocity (Fig. S6 left, ESI†). Thermal imaging confirms the subjective observation of particles slowing down the propagating front. Both samples filled with 1 vol% of silica yield a similar drop in front velocity. It falls by 25–28% from 3.2 mm s^{-1} for the unfilled formulation to 2.3 and 2.4 mm s^{-1} for 14 nm and 200–300 nm particles, respectively. Polymer-adsorbing particles contribute to the physical cross-linking.[35] Higher cross-linking density slows down the diffusion and, thus, the front propagation.[2] However, scaling with the particle size and surface area would be expected in such a case, which contradicts the current results.

The front temperature (Fig. S6 right, ESI†) is calculated from the average maximum temperature recorded by the thermal camera at the steady front propagation phase (Fig. 4 left). We note that the spatial resolution of thermal imaging is insufficient to evaluate the temperature of individual particles. Moreover, no other technique known to authors is available to monitor temperature profiles at nanoscale precision inside the formulation during the reaction. Therefore, no local temperature variation near the silica surface was considered. The front head of the 3% IOC formulation raises the temperature from ambient conditions (~18 °C) to the maximum of 253.9 °C in about 6–7 s. Silica reduces the front temperature to 236.7 and 238.6 °C mm s^{-1} for 14 nm and 200–300 nm particles, respectively (Fig. S6 right, ESI†). The drop by 17.2/15.3 °C corresponds to roughly 7% of the total temperature change experienced at the front head (~234 °C).

The recorded front temperatures mismatch the expectation based on the M-DSC measurement (Fig. 3), where the filled samples produce larger excess enthalpy. This observation might be partially related to the M-DSC experimental setup, which falls out of the FP conditions, and the heat distribution around the front, as our further results suggest.

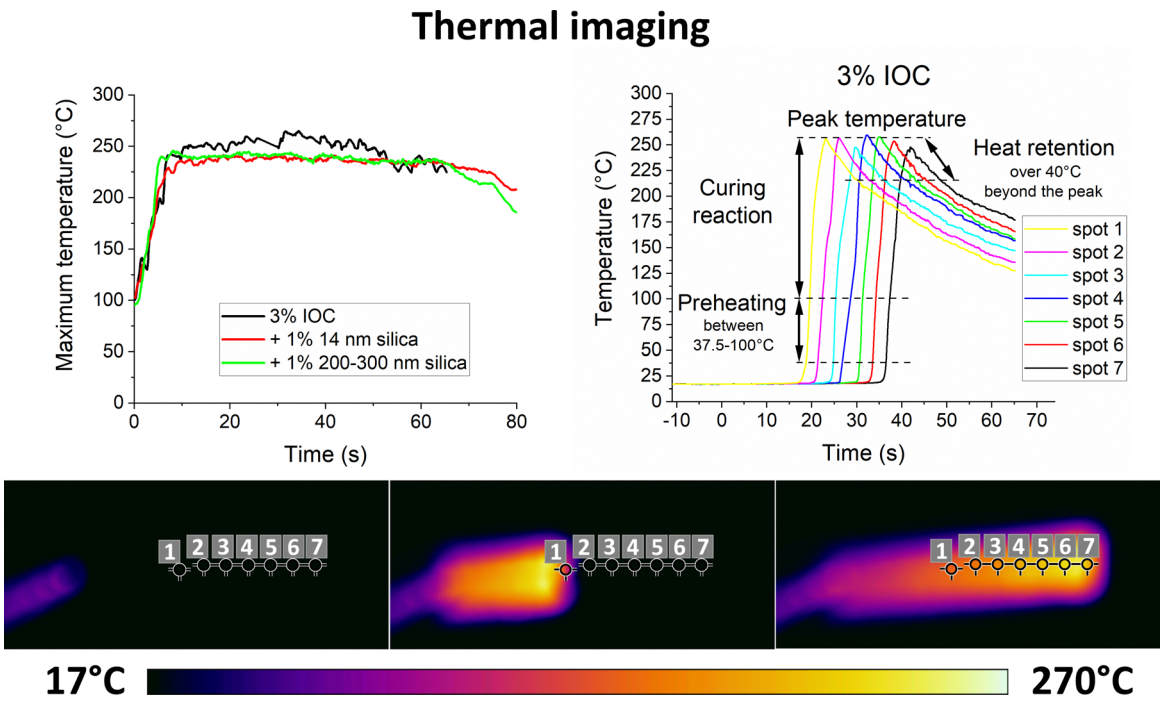

Fig. 4 Maximum temperature (top left) and temperature profiles of the neat unfilled 3% IOC sample at selected fixed points (top right) of the frontal polymerization recorder by thermal imaging (bottom). Temperature profiles of the filled samples can be found in Fig. S5 (ESI†).

The initial heating rate ahead of the front (Fig. S7 left, ESI†) is evaluated in the range of 37.5–100 °C according to the M-DSC results (Fig. 3). While the unfilled formulation heats up at the rate of 86.6 °C s^{-1}, the silica-filled samples show the rate of 48.1 and 53.3 °C s^{-1} for the 14 nm and 200–300 nm particles, respectively. This variation by 44.5/38.5% exceeds the simple expectation based on the different front velocities where the change caused by particles is only 25–28% (Fig. S6 left, ESI†). It suggests that the silica-filled formulations start to preheat further ahead of the front, thus, heating a larger volume while consuming more heat from the front head.

The post-curing curves are fitted with a linear regression at 40 °C beyond the peak temperature (Fig. S7 right, ESI†). This approach might be a little oversimplistic, yet it provides a single-parameter characteristic that could be easily used to compare different samples. The 3% IOC, 1 vol% silica 14 nm, and 1 vol% silica 200–300 nm samples' cooling rates are 4.2, 2.2, and 2.4 °C s^{-1}, respectively. Hence, the slower cooling rate of the filled formulations further restrains the front head from the heat supply since it is more retained behind the front.

Finally, we tested whether the shear gradient at the front head could push particles. This could increase the particles' local concentration ahead of the front and magnify the particle-induced effects. Therefore, several specimens collected from sites of an FP sample at varying distances from the initiation point are tested by TGA (Fig. S7, ESI†). The residual weights are corrected by the residual weight of unfilled matrix reference and recalculated to volume ratios according to the silica density. No significant variation in particle concentration is found for either 14 nm or 200–300 nm particles, suggesting no such effect taking place regardless of the particle size (Fig. S7, ESI†).

4. Conclusion

Adding particles to a FP formulation may require adjustments to maintain the frontal regime of polymerization. Either the formulation could be preheated before the initiation, the reaction rate can be accelerated by adding more initiator, or the reaction enthalpy might be increased by adjusting the monomer composition. The lower reaction enthalpy of the filled samples is countered by their reduced heat capacity, leading to a greater excess enthalpy as recorded by modulated DSC. On the other hand, thermal imaging reveals slower preheating, front propagation, and cooling rates of the filled formulations. It suggests that the excess energy spread into a larger area/volume ahead of the front while more heat is retained behind it.

These results follow the same trend as the change in front temperature and velocity, yet the rate varied by a different relative ratio than the other properties. It suggests that the front velocity is not the only contribution to the other changes. Finally, the front capability to push particles was tested with no evidence for such behavior. The current results set up essential narratives for the design and practical applications of frontally polymerized foams with non-reactive fillers. Further work shall focus on the anisotropic properties of these materials and the morphological changes caused by the particular fillers.

Conflicts of interest

A patent WO 2022/087097 A1 owned by BASF company and the University of Massachusetts Amherst protects the basic FP foam formulation.

Acknowledgements

This work was supported by the Frontal Polymerization for Microcellular Foams (NORA) project supported by BASF company through the Northeast Research Alliance (NORA). P. Lepcio acknowledges the GF21-43070L project supported by GA ČR.

References

1 Q. Li, H.-X. Shen, C. Liu, C.-F. Wang, L. Zhu and S. Chen, Advances in Frontal Polymerization Strategy: From Fundamentals to Applications, *Prog. Polym. Sci.*, 2022, **127**, 101514, DOI: **10.1016/j.progpolymsci.2022.101514**.

2 H. Liu, H. Wei and J. S. Moore, Frontal Ring-Opening Metathesis Copolymerization: Deviation of Front Velocity from Mixing Rules, *ACS Macro Lett.*, 2019, **8**(7), 846–851, DOI: **10.1021/acsmacrolett.9b00367**.

3 I. D. Robertson, M. Yourdkhani, P. J. Centellas, J. E. Aw, D. G. Ivanoff, E. Goli, E. M. Lloyd, L. M. Dean, N. R. Sottos, P. H. Geubelle, J. S. Moore and S. R. White, Rapid Energy-Efficient Manufacturing of Polymers and Composites via Frontal Polymerization, *Nature*, 2018, **557**(7704), 223–227, DOI: **10.1038/s41586-018-0054-x**.

4 Y. Cui, J. Yang, Y. Zhan, Z. Zeng and Y. Chen, In Situ Fabrication of Polyacrylate/Nanozirconia Hybrid Material via Frontal Photopolymerization, *Colloid Polym. Sci.*, 2008, **286**(1), 97–106, DOI: **10.1007/s00396-007-1752-3**.

5 D. M. Alzate-Sanchez, M. M. Cencer, M. Rogalski, M. E. Kersh, N. Sottos and J. S. Moore, Anisotropic Foams via Frontal Polymerization, *Adv. Mater.*, 2022, **34**(8), 2105821, DOI: **10.1002/adma.202105821**.

6 J. D. Mota-Morales, R. J. Sánchez-Leija, A. Carranza, J. A. Pojman, F. del Monte and G. Luna-Bárcenas, Free-Radical Polymerizations of and in Deep Eutectic Solvents: Green Synthesis of Functional Materials, *Prog. Polym. Sci.*, 2018, **78**, 139–153, DOI: **10.1016/j.progpolymsci.2017.09.005**.

7 N. P. Totaro, Z. D. Murphy, A. E. Burcham, C. T. King, T. F. Scherr, C. O. Bounds, V. Dasa, J. A. Pojman and D. J. Hayes, In Vitro Evaluation of Thermal Frontally Polymerized Thiol-ene Composites as Bone Augments, *J. Biomed. Mater. Res., Part B*, 2016, **104**(6), 1152–1160, DOI: **10.1002/jbm.b.33466**.

8 E. Goli, N. A. Parikh, M. Yourdkhani, N. G. Hibbard, J. S. Moore, N. R. Sottos and P. H. Geubelle, Frontal Polymerization of Unidirectional Carbon-Fiber-Reinforced Composites, *Composites, Part A*, 2020, **130**, 105689, DOI: **10.1016/j.compositesa.2019.105689**.

9 L. Chen, T. Hu, H. Yu, S. Chen and J. A. Pojman, First Solvent-Free Synthesis of Poly(N-Methylolacrylamide) via Frontal Free-Radical Polymerization, *J. Polym. Sci., Part A: Polym. Chem.*, 2007, **45**(18), 4322–4330, DOI: **10.1002/pola.22176**.

10 J. A. Pojman, G. Gunn, C. Patterson, J. Owens and C. Simmons, Frontal Dispersion Polymerization, *J. Phys. Chem. B*, 1998, **102**(20), 3927–3929, DOI: **10.1021/jp9814911**.

11 A. Mariani, S. Fiori, S. Bidali, V. Alzari and G. Malucelli, Frontal Polymerization of Diurethane Diacrylates, *J. Polym. Sci., Part A: Polym. Chem.*, 2008, **46**(10), 3344–3352, DOI: **10.1002/pola.22675**.

12 B. Wang, B. Yin, Z. Zhang, Y. Yin, Y. Yang, H. Wang, T. P. Russell and S. Shi, The Assembly and Jamming of Nanoparticle Surfactants at Liquid–Liquid Interfaces, *Angew. Chem., Int. Ed.*, 2022, **61**(10), e2021149, DOI: **10.1002/anie.202114936**.

13 Y. Li, R. K. Kankala, Z. Weng and L. Wu, Dual-Cure Vapor-Grown Carbon Nanofiber-Supplemented 3D-Printed Resin: Implications for Improved Stiffness and Thermal Resistance, *ACS Appl. Nano Mater.*, 2022, **5**(7), 9544–9553, DOI: **10.1021/acsanm.2c01774**.

14 I. M. Factori, J. M. Amaral, P. H. Camani, D. S. Rosa, B. A. Lima, M. Brocchi, E. R. da Silva and J. S. Souza, ZnO Nanoparticle/Poly(Vinyl Alcohol) Nanocomposites via Microwave-Assisted Sol–Gel Synthesis for Structural Materials, UV Shielding, and Antimicrobial Activity, *ACS Appl. Nano Mater.*, 2021, **4**(7), 7371–7383, DOI: **10.1021/acsanm.1c01334**.

15 S. Kumar, G. Saeed, L. Zhu, K. N. Hui, N. H. Kim and J. H. Lee, 0D to 3D Carbon-Based Networks Combined with Pseudocapacitive Electrode Material for High Energy Density Supercapacitor: A Review, *Chem. Eng. J.*, 2021, **403**, 126352, DOI: **10.1016/j.cej.2020.126352**.

16 T. Xu, H. Du, H. Liu, W. Liu, X. Zhang, C. Si, P. Liu and K. Zhang, Advanced Nanocellulose-Based Composites for Flexible Functional Energy Storage Devices, *Adv. Mater.*, 2021, **33**(48), 2101368, DOI: **10.1002/adma.202101368**.

17 S. P. Davtyan, A. A. Berlin, K. Shik, A. O. Tonoyan and S. Z. Rogovina, Polymer Nanocomposites with a Uniform Distribution of Nanoparticles in a Polymer Matrix Synthesized by the Frontal Polymerization Technique, *Nanotechnol. Russ.*, 2009, **4**(7–8), 489–498, DOI: **10.1134/S1995078009070106**.

18 M. S. Abzan, R. Mirzaee, S. Ahmadi, N. Karimpour-Motlagh and H. A. Khonakdar, Affected Polymer Layer and Thermo-Mechanical Behavior Correlation in Nylon-6/Polycarbonate/Graphene-Oxide Nanocomposites: A Quantitative Study of Polymorphism, *Thermochim. Acta*, 2021, **703**, 178995, DOI: **10.1016/j.tca.2021.178995**.

19 K. Zarybnicka, F. Ondreas, P. Lepcio, M. Kalina, M. Zboncak and J. Jancar, Thermodynamic Parameters Controlling Nanoparticle Spatial Packing in Polymer Solutions, *Macromolecules*, 2020, **53**(19), 8704–8713, DOI: **10.1021/acs.macromol.0c00698**.

20 P. Lepcio, F. Ondreáš, K. Zárybnická, M. Zbončák, J. Svatík and J. Jančář, Phase Diagram of Bare Particles in Polymer

Nanocomposites: Uniting Solution and Melt Blending, *Polymer*, 2021, **230**, 124033, DOI: 10.1016/j.polymer.2021.124033.

21 Y. Sui, Y. Cui, X. Meng and Q. Zhou, Research Progress on the Correlation between Properties of Nanoparticles and Their Dispersion States in Polymer Matrix, *J. Appl. Polym. Sci.*, 2022, **139**(19), 52096, DOI: 10.1002/app.52096.

22 F. Ondreas, P. Lepcio, M. Zboncak, K. Zarybnicka, L. E. Govaert and J. Jancar, Effect of Nanoparticle Organization on Molecular Mobility and Mechanical Properties of Polymer Nanocomposites, *Macromolecules*, 2019, **52**(16), 6250–6259, DOI: 10.1021/acs.macromol.9b01197.

23 A. Ghanekarade, A. D. Phan, K. S. Schweizer and D. S. Simmons, Nature of Dynamic Gradients, Glass Formation, and Collective Effects in Ultrathin Freestanding Films, *Proc. Natl. Acad. Sci. U. S. A.*, 2021, **118**(31), e21043 98118, DOI: 10.1073/pnas.2104398118.

24 V. Bernardo, F. Loock, J. Martin-de Leon, N. A. Fleck and M. A. Rodriguez-Perez, Mechanical Properties of PMMA-Sepiolite Nanocellular Materials with a Bimodal Cellular Structure, *Macromol. Mater. Eng.*, 2019, **304**(7), 1900041, DOI: 10.1002/mame.201900041.

25 S. Costeux and L. Zhu, Low Density Thermoplastic Nanofoams Nucleated by Nanoparticles, *Polymer*, 2013, **54**(11), 2785–2795, DOI: 10.1016/J.POLYMER.2013.03.052.

26 P. Lepcio, J. Svatík, M. Štaffová, A. J. Lesser and F. Ondreáš, Revealing the Combined Nanoconfinement Effect by Soft and Stiff Inclusions in PMMA/Silica CO2 Blown Foams, *Macromol. Mater. Eng.*, 2022, **307**(11), 2200403, DOI: 10.1002/mame.202200403.

27 A. Kausar, Advances in Polymer-Anchored Carbon Nanotube Foam: A Review, *Polym. Technol. Mater.*, 2019, **58**(18), 1965–1978, DOI: 10.1080/25740881.2019.1599945.

28 P. Lepcio, J. Svatík, E. Režnáková, D. Zicha, A. J. Lesser and F. Ondreáš, Anisotropic Solid-State PLA Foaming Templated by Crystal Phase Pre-Oriented with 3D Printing: Cell Supporting Structures with Directional Capillary Transfer Function, *J. Mater. Chem. B*, 2022, **10**(15), 2889–2898, DOI: 10.1039/D1TB02133H.

29 M. Štaffová, F. Ondreáš, J. Svatík, M. Zbončák, J. Jančář and P. Lepcio, 3D Printing and Post-Curing Optimization of Photopolymerized Structures: Basic Concepts and Effective Tools for Improved Thermomechanical Properties, *Polym. Test.*, 2022, **108**, 107499, DOI: 10.1016/j.polymertesting.2022.107499.

30 F. Fraga, C. Castro-Diaz, E. Rodriguez-Núñez and J. M. Martinez-Ageitos, Physical Aging for an Epoxy Network Diglycidyl Ether of Bisphenol A/m-Xylylenediamine, *Polymer*, 2003, **44**(19), 5779–5784, DOI: 10.1016/S0032-3861(03)00624-4.

31 K. Zarybnicka, P. Lepcio, J. Svatik, J. Jancar and F. Ondreas, Effect of the Nanoparticles on the Morphology and Mechanical Performance of Thermally Blown 3D Printed HIPS Foams, *J. Appl. Polym. Sci.*, 2023, **140**(5), e53413, DOI: 10.1002/app.53413.

32 M. Korčušková, V. Sevriugina, F. Ondreáš, J. Svatík, W. Tomal, V. Vishakha, J. Ortyl and P. Lepcio, Photoactivity, Conversion Kinetics, Nanoreinforcement, Post-Curing, and Electric/Dielectric Properties of Functional 3D Printable Photopolymer Resin Filled with Bare and Alumina-Doped ZnO Nanoparticles, *Polym. Test.*, 2022, **116**, 107798, DOI: 10.1016/j.polymertesting.2022.107798.

33 R. S. Drago, G. C. Vogel and T. E. Needham, Four-Parameter Equation for Predicting Enthalpies of Adduct Formation, *J. Am. Chem. Soc.*, 1971, **93**(23), 6014–6026, DOI: 10.1021/ja00752a010.

34 Y. Yang, H. Zhang, P. Wang, Q. Zheng and J. Li, The Influence of Nano-Sized TiO_2 Fillers on the Morphologies and Properties of PSF UF Membrane, *J. Memb. Sci.*, 2007, **288**(1–2), 231–238, DOI: 10.1016/j.memsci.2006.11.019.

35 A. C. Yu, H. Lian, X. Kong, H. Lopez Hernandez, J. Qin and E. A. Appel, Physical Networks from Entropy-Driven Non-Covalent Interactions, *Nat. Commun.*, 2021, **12**(1), 746, DOI: 10.1038/s41467-021-21024-7.

